Applied Surface Science Advances 20 (2024) 100581

Contents lists available at ScienceDirect

Applied Surface Science Advances

journal homepage: www.sciencedirect.com/journal/applied-surface-science-advances

An experimental and theoretical aided 2D MoS_2 nanoflowers strategy for rapid visual sensing of Gallic acid in food and clinical matrixes

Aizaz Khan [a], Huma Ajab [a,*], Asim Yaqub [b], Khurshid Ayub [a], Muhammad Yar [a], Habib Ullah [c]

[a] Department of Chemistry, COMSATS University Islamabad, Abbottabad Campus, Pakistan
[b] Department of Environmental Sciences, COMSATS University Islamabad, Abbottabad Campus, Pakistan
[c] College of Engineering, Mathematics and Physical Sciences, University of Exeter, Penryn Campus, Cornwall TR10 9FE, United Kingdom

ARTICLE INFO

Keywords:
Sensor
Colorimetric
Gallic acid
Food
Environment
DFT
MoS_2

ABSTRACT

Gallic acid (GA), an important phenolic component, is gaining popularity due to its biological and industrial applications. However, its rapid expansion can be hazardous, causing cancer and gene damage, making the design of a low-cost and fast GA sensor difficult. We used a single-step hydrothermal approach to synthesize MoS_2 nanoparticles for colorimetric detection of GA. The nanoparticles were analyzed using techniques like; UV–Vis spectroscopy, FT-IR spectroscopy, SEM, EDX and XRD. The optimization of key parameters such as MoS_2 concentration (2.0 mg), temperature (30 °C), and pH (7) resulted in a limit of detection (LOD) of 0.125×10^{-6} M with a dynamic range of 0.5 to 36×10^{-6} M. MoS_2 nanoflowers performed as nanozymes in the filter paper-based sensor, catalyzing 3, 3′, 5, 5′-tetramethylbenzidine (TMB) oxidation, while GA acted as an inhibitor to prevent further reaction progression. The detection was made feasible through capturing an image support by an ordinary smartphone and the steady-state kinetic study validated MoS_2 nanoflowers' affinity for sensing H_2O_2. The sensor performed well in real-world samples such as diet tea, green tea, water, blood serum, and urine, with recovery rates ranging from 93.2 % to 102.1 %. Density functional theory calculations were applied to provide an insight into GA-MoS_2 binding interactions and changes in electronic properties. With all of these merits, we believe MoS_2 nanoparticles can provide low-cost and portable filter paper-based strips as a sensing platform for visual assessment of GA.

1. Introduction

Gallic acid (GA) is a benzoic acid that occurs naturally in phenolic compounds such as green tea, banana leaves, black rice, and blueberries. It is widely utilized in a variety of key industries such as pharmaceuticals, foods, cosmetics, lipids, oils, ink, dye, and so on [1]. GA has excellent antioxidant capabilities and is also antiviral, antiradical, antibacterial, antimutagenic, anticancer, anti-inflammatory, and cardiovascular protective [2]. It has been implicated in the reduction of mitochondrial dysfunction and has a substantial neuroprotective consequence on cerebral ischemia. Aside from medicine, GA plays an essential role in a variety of critical industries, such as serving as a preservation agent in food and drinks owing to its aptitude to capture free radicals [3]. However, in addition to its vital applications, its quantification is very important to control the quality of GA-based medications and other health-care products. Its long term intake in *vivo* by the human is very toxic even at low concentrations due to its poor biodegradability nature in water. Rising levels of GA due to regular intake in the body can cause cancer, disrupt DNA sequences, and cause other major concerns. Along with it carcinogenic effect, the recent study also reported that the GA produces the reactive oxygen species (ROS) which induces apoptosis the cultures of cancer cells [4].

As a result, there is an immense demand for an effective and selectively valid analytical instrument that can quickly assess the GA in a real medium. Several traditional analytical approaches are being used for its detection, including high-performance liquid chromatography (HPLC) [5], spectrophotometry [6], flow injection analysis [7]. MnO_2-based POD was a platform used before for the spectrophotometric valuation of antioxidant behaviors of natural antioxidants. Antioxidants are reductants that can eliminate the active oxygen species or the free radicals produced in organisms [8]. These techniques are very selective, but they have some major constraints, such as trained personnel, extensive procedures, and expensive equipment. On the contrary, colorimetric sensing techniques are presently regarded as the most appropriate and

* Corresponding author.
E-mail address: humaajab@cuiatd.edu.pk (H. Ajab).

https://doi.org/10.1016/j.apsadv.2024.100581
Received 27 November 2023; Received in revised form 11 January 2024; Accepted 15 February 2024
Available online 24 February 2024

effective tools due to several of their distinctive leads such as low cost, great selectivity and sensitivity, simple setup and fast measurement time. In comparison to other sensing techniques, the filter paper-based colorimetric assay has the benefit of allowing detection to be observed with the naked eye by changing the color. Color signaling is a preferred option in traditional visual sensing owing to its simplicity and broad applicability [9].

Colorimetric detection has recently been widely used for the exposure of a variety of important analytes, including DNA, proteins, heavy metals [10], oxalate [11] and others. Most of the currently known colorimetric methods for GA detection use peroxidase enzymes to catalyze the appropriate enzymatic chromogenic substrate (TMB) for the formation of a blue signal product.

In the domain of colorimetric sensing, the practice of nanoparticles as a substitute for natural enzymes for catalyzing diverse reactions has sparked considerable attention in recent years. This is because inherent limitations associated with natural enzymes, such as their high cost, low stability, and struggle in bulk manufacturing, hinders their advancement in applications [12].

There are widely used applications of natural enzymes in the fields of medical sciences, environmental control, fermentation industries, and synthesis biology because of their excellent catalytic activities. Beside of their broad applications, several serious limitations including difficulty in recycling, high cost and minimum stability suppress their uses. To get around these issues, the enzyme mimic takes their place [13]. Nanozymes, which are based on nanomaterials that mimic the functions of enzymes, have sparked a great deal of interest in research due to their excellent biocompatibility, adaptability, chemical stability, and enzyme activities. They are also widely used as antibacterial agents in a variety of therapeutic contexts and for biosensing applications. Among these are enzyme mimicking nanostructures or composites based on transition metals such as MoS_2, Co-MoS_2 and Co_3O_4 performing enzyme mimic behavior's [14]. Numerous enzyme mimetics have been synthesized based on different nanoparticles, like gold (Au), platinum (Pt), metal oxides, including iron oxide (Fe_3O_4), magnetized nanocomposite of *Pinus* [15], cerium oxide (CeO_2) [16], carbon-based nanomaterials like fullerenes and carbon dots [17], which have good peroxidase-like properties. Compared to horseradish peroxidase (HRP), these peroxidase mimics are extremely essential due to lower prices, greater design freedom, and improved chemical stability. Molybdenum disulfide and graphene (oxide) have been mentioned among these peroxidase mimics owing to their good peroxidase mimic properties [18].

The class of metal oxides has many uses in gas-related sensors in the current decade because of some of its appealing characteristics, such as good sensitivity, simple structure, and great flexibility. However, a few significant drawbacks, such as high power consumption and operating temperature, restrict the applications that may be used with it [19]. MoS_2, a two-dimensional (2D) layered transition metal dichalcogenides material with special optical, electrical, and mechanical properties similar to graphene, has been gaining prominence recently [20]. MoS_2 has engrossed attention due to its exceptional physical features, particularly its complimentary electrical behavior, and its widespread use in transistors, sensors, optoelectronics, and electroluminescent devices [21]. MoS_2 has been extensively studied in sensing applications like; Lin et al. described the naked eye glucose detection by means of MoS_2 nanoparticles [22]. Wang and colleagues reported work on nanocomposite of 3D graphene/Fe_3O_4 with good nanozyme action for glucose sensing [23]. Despite substantial developments in nanostructured artificial enzymes, there is still a demand for cost-effective, stable peroxidase mimics with quick and high catalytic performance, particularly in real-world environments.

Theoretical studies, on the other hand, when supplemented with experimentation methodologies, can provide insight into the interaction between the material and the desired analyte. Density functional theory (DFT) calculations offer theoretical insight into sensing mechanisms by calculating the electronic structure and energy of the system, including the analyte and sensor material. DFT can reveal a sensor's properties while decreasing the amount of material and nanopowder required for the experiment. Tang synthesized a nanocomposite on the basis of transition metal-doped MoS_2 by following solvothermal route, by applying DFT calculation with their experiments, it was concluded that the sensor have a fast recovery time/response time, excellent stability, and maximum response value to NO_2 [24]. Zhang et al. established their sensing mechanism and the impact of various crystal planes on the detection properties of ammonia by using the DFT calculations [25]. Liu et al. with the help DFT calculation explored the adsorption of byproduct resulting from the decomposition of SF_6 on WSe_2 (with TM replacement and atoms) modified on transition metals (Ag, Pt, Pd, Rh and Ru) [26]. The density of states (DOS) analysis illustrates how the electronic states are perturbed by the interaction of the analyte with the substrate, allowing for understanding the strength of the interaction and estimating recovery time.

To solve the aforementioned constraints, the current study was carried out, which was based on 2D-nanoparticles of MoS_2 as a visual paper strip platform for the rapid detection of GA. Therefore, a new application of MoS_2 nanoflowers for the detection of GA in food and clinical samples has been proposed, validating its potential for direct visual food quality monitoring. To strengthen the computational conclusions, we also integrated experimental data with computing results from density functional theory in our work. This new study domain provides a fascinating path for figuring out the complexities of GA's interaction with colorimetric sensor devices, potentially yielding novel insights into the optical responses induced by such interactions.

Following a single-step hydrothermal synthesis technique, characterization studies such as UV–Vis spectroscopy, fourier-transform infrared spectroscopy (FT-IR), scanning electron microscope (SEM), energy dispersive X-ray (EDX) and X-Ray diffraction (XRD) were conducted. Several factors, including concentration (material and TMB), temperature, and pH, were optimized. Besides, selectivity and sensitivity tests were carried out in order to determine the figure of merits. Kinetic elucidations were also carried out, and the mechanism was thoroughly defined. DFT calculations were performed to gain insight into the binding interactions of GA with MoS_2, as well as fluctuations in electronic characteristics. Real-world applications were successfully carried out to test the proposed sensor's direct onsite monitoring capability and portability.

2. Materials and methods

2.1. Chemicals and reagents

Ammonium molybdate ($(NH_4)_6Mo_7O_{24}$) (99.98 %) and thiourea (CH_4N_2S) (99 %) were purchased from DAEJUNG, 3,3′,5,5′-tetramethylbenzidine (TMB) (99.6 %), ethanol (96 %), sodium alginate $(C_6H_7NaO_6)_n$ (≥99 %), maltose ($C_{12}H_{22}O_{11}$) ≥99.0 %, L-alanine ($C_3H_7NO_2$) (99 %), glycine ($C_2H_5NO_2$) (99 %), dopamine ($C_8H_{11}NO_2$) (≥98 %), pyrocatechol ($C_6H_6O_2$) (≥99 %), uric acid ($C_5H_4N_4O_3$), citric acid ($C_6H_8O_7$) (≥99.5 %), hydrogen peroxide (H_2O_2) (30.1 %), ascorbic acid ($C_6H_8O_6$) besides sodium hydroxide (NaOH) (≥99 % purity) were obtained from Sigma Aldrich. Diet tea and green tea were bought at a local market in Abbottabad, Pakistan, and urine and blood samples were acquired from a regional medical laboratory Abbottabad, Pakistan. Distilled water (DW) was used to make all of the solutions in this study.

2.2. Instrumentations and characterization techniques

An electronic balance from K. Roy (Model number 108), a magnetic stirrer/hot plate from Abron Exports (Model number MSWHP), and a pH meter (Starter 3100, OHAUS) were used for weighing, stirring, and adjusting of pH. The synthesized material was characterized consuming a variety of appropriate analytical techniques, including a UV–visible spectrophotometer ((Specord 200+ of Analytik Gena's, serial no.

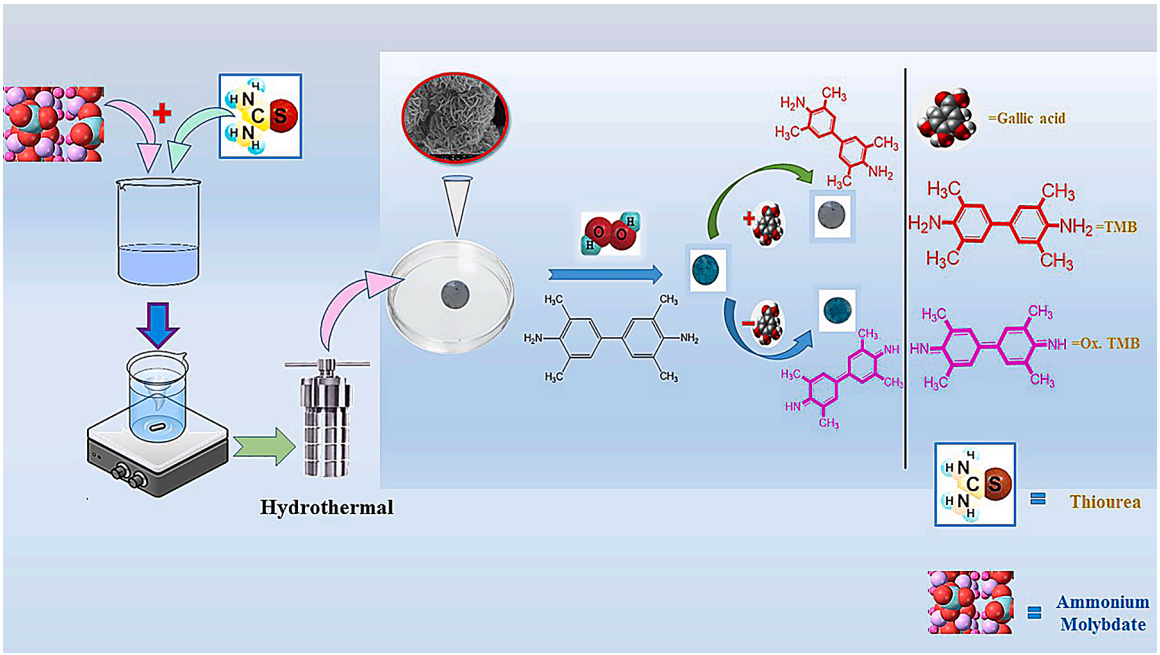

Fig. 1. Graphical illustration for the synthesis of MoS_2 nanoflowers and strategy of GA detection.

223E2003C, Germany)) in the wavelength range of 200 - 800 nm, scanning electron microscopy (SEM) and energy dispersive X-ray (EDX) (JSM5910, JEOL, Japan) was used to identify the external structure and elemental conformation of the synthesized material, and XRD (JDX 3532, JEOL, Japan) was used to assess the crystal size of the applied material in 2θ ranges of 10–80° and 20–40 kV, while Fourier transform infrared spectroscope (FT-IR) (Shimadzu FTIR-8400S Spectrum) was used to find out functional groups of the MOS_2 (range =3000 to 500 cm^{-1}).

2.3. Software/Statistical analysis

The RGB values were calculated using Image J software by taking averages. For the graphs, Origin software (version 2022) was used, Xpert High Score Plus (PAN analytical version 3.0) was applied for plotting of XRD data, and End Note X8.0.2 was used for article citation. The filter paper images were captured using a Tecno with a 16-megapixel depth sensor, which was ideal for producing high-quality images.

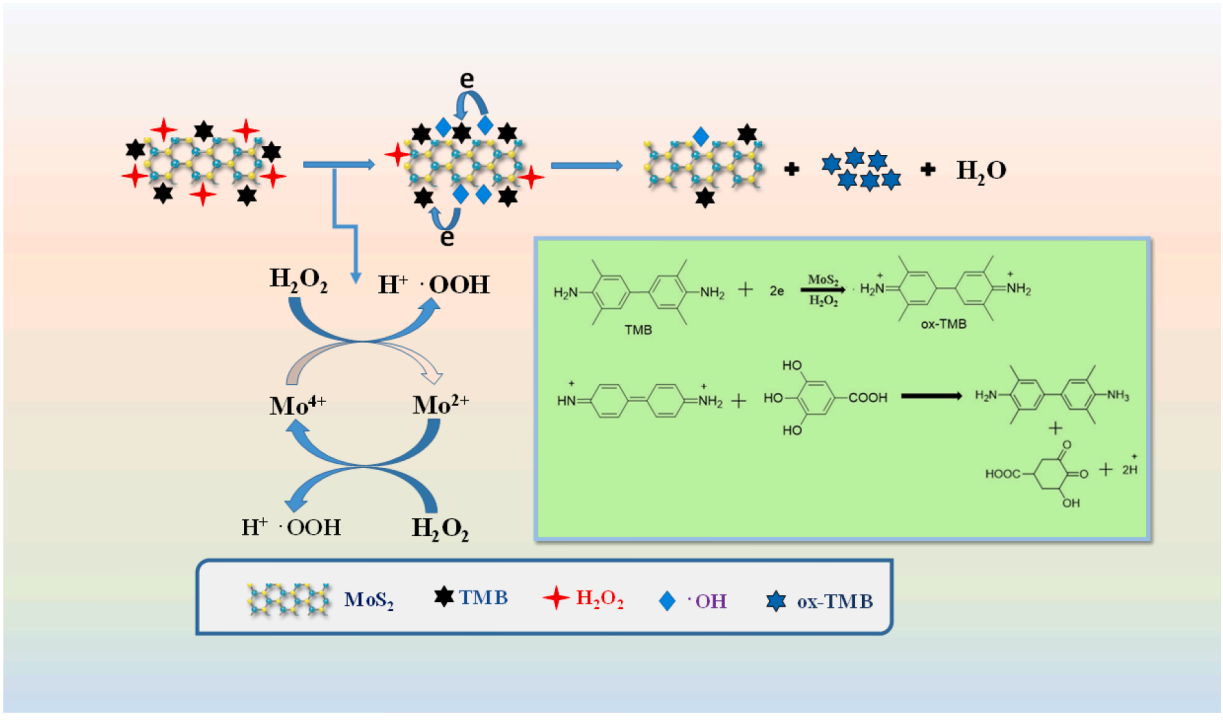

Scheme 1. Mechanism of GA detection based on the catalytic impact of MoS_2 nanoflowers.

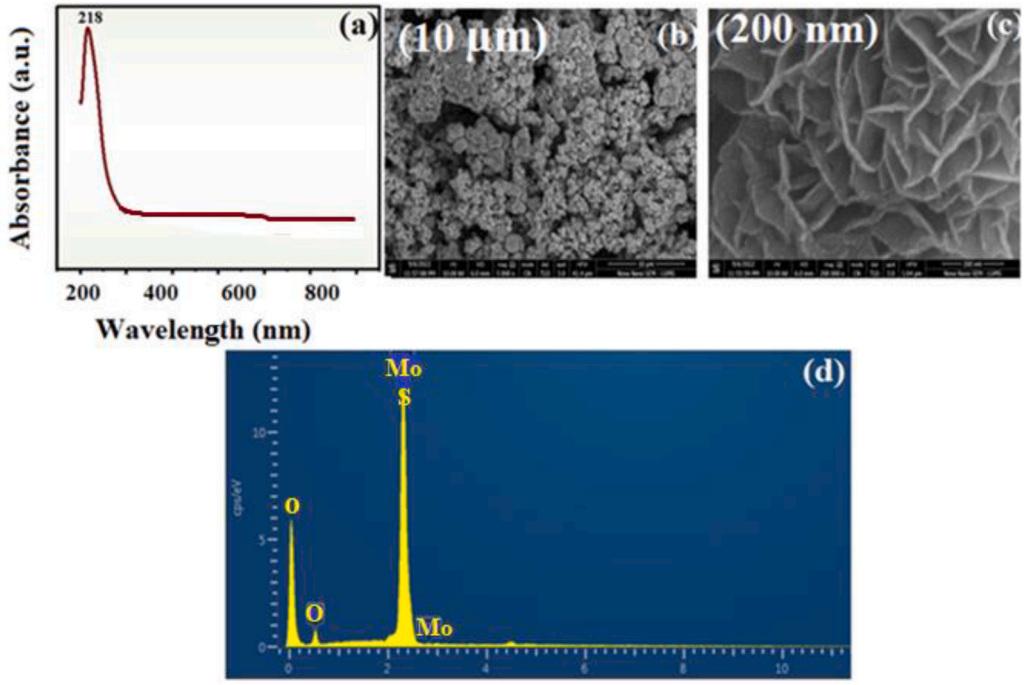

Fig. 2. (a) UV- Visible absorption spectrum of MoS_2 nanoflowers, (b) SEM image of MoS_2 nanoflowers at 10 µm, (c) 200 µm, (d) EDX spectrum of MoS_2 nanoflowers.

2.4. Hydrothermal synthesis of molybdenum disulphide (MoS_2)

MoS_2 nanoparticles were synthesized using a simple and single-stage hydrothermal method [27], as shown in Fig. 1. Briefly, 0.8 g of $(NH_4)_6Mo_7O_{24}$ and 5.12 g of CH_4N_2S were dissolved in 80 mL of DI water with constant stirring to generate a clear solution. The produced solution was then shifted to an autoclave and heated at 200 °C for 16 h. The resulting black precipitates were sprinkled several times with 70 % C_2H_5OH before drying in an oven at 70 °C for 12 h. Finally, the blackish-colored MoS_2 nano-powder was collected and applied for the desired work.

2.5. Fabrication of a colorimetric sensor and mechanism of the MoS_2 nanoflowers in an H_2O_2-TMB system

A petri dish containing 0.3 g/6 mL of sol-gel and 3 mg of MoS_2 nanopowder was used to fabricate a colorimetric sensor on the surface of filter paper. In brief, a nanoparticle and sodium alginate gel mixture was poured onto the surface of a 0.6 mm diameter filter paper. The proposed colorimetric sensor based on filter paper was utilized to track and monitor GA using portable colorimetric assays. A colorimetric reaction with TMB as the chromogenic substrate was used to determine MoS_2's peroxidase-like activity.

To start with, the influence of temperature, material, pH, and H_2O_2 concentrations on MoS_2 peroxidase-like activity was examined in order to find the best operating settings for the MoS_2 sensing system. For color quantification and intensity measurements, a high-resolution smartphone camera was set up at a distance of 10 cm from each filter paper. Image J software with three different colors (blue, green, and red) was used to evaluate the output signal of each filter paper in order to analyze color intensity. It was used because its simplicity and support for displaying images via PC and LCDs, and these analyses were performed based on image color intensity. Based on the analysis software results for the acquired filter paper images, a calibration curve was generated that reflects the colorimetric illustration of the proposed sensor platform.

Scheme 1 demonstrated the catalytic process of MoS_2 nanoflowers, the H_2O_2 molecules were initially adsorbed on the surface of MoS_2 nanoflowers, where the Mo^{4+} center immediately activated them to create highly reactive hydroxyl species (•OH). TMB was then oxidized by the hydroxyl species, yielding an oxidized TMB (ox-TMB) [28]. Furthermore, the configuration of MoS_2 nanoparticles improved the specific surface area, which made it ideal for the enrichment of H_2O_2 and TMB onto its surface. Additionally, the MoS_2 nanoflowers displayed high peroxidase-like activity in the manifestation of H_2O_2 via accelerating TMB oxidation, as evidenced by the appearance of a blue color from a colorless one when observed with the naked eye. The antioxidant GA induced two electrons for the conversion of ox-TMB to TMB, resulting in the solution's blue hue fading.

In order to further understand the reaction mechanism, the literature reported about the electronic spin resonance (ESR) measurement techniques for the further explanation of the oxidase-like activity. The MoS_2 catalytic mechanism may be considered as the participation of reactive oxygen species (ROS) produced during the reaction process by the activation of oxygen (O_2) species. The oxygen vacancies ($h+$), hydroxyl radicals (•OH), singlet oxygen ($^1O_2$) and superoxide anions ($O_2^{\cdot -}$) are individually collected by the sacrificial agents including EDTA, BQ, NAN_3 and TBA. After the introduction of H_2O_2, the applied TMB become oxidized owing to the production of •OH ions. When H_2O_2 came in contact to MoS_2 nanoflowers, the p-orbital electron of the O atom in the H_2O_2 migrated to the d-orbital of the Mo atom, leading the interaction among the MoS_2 and the applied H_2O_2. Now, the O_2 was excluded from the reaction system and the further production of $O_2^{\cdot -}$ and $^1O_2$ became disturbed. As the result, the peroxidase-mimic activities of the applied MoS_2 nanomaterials became enhanced owing by •OH ions which was generated in the presence of H_2O_2. Taking together, following the targeted suppression of oxidase-like activity through the addition of EDTA, the MoS_2 nanoflowers acted as outstanding and specific peroxidase mimics by catalyzing the •OH ions during the reaction [29–31].

2.6. Computational methodology

The density functional calculations for geometric relaxation and electronic properties were performed by Quantum Espresso code. The general gradient approximation (GGA) method with Perdew-Burke Ernzerhof (PBE) parameterization was employed to approximate electron exchange-correlation functional. Geometry optimization and elec-

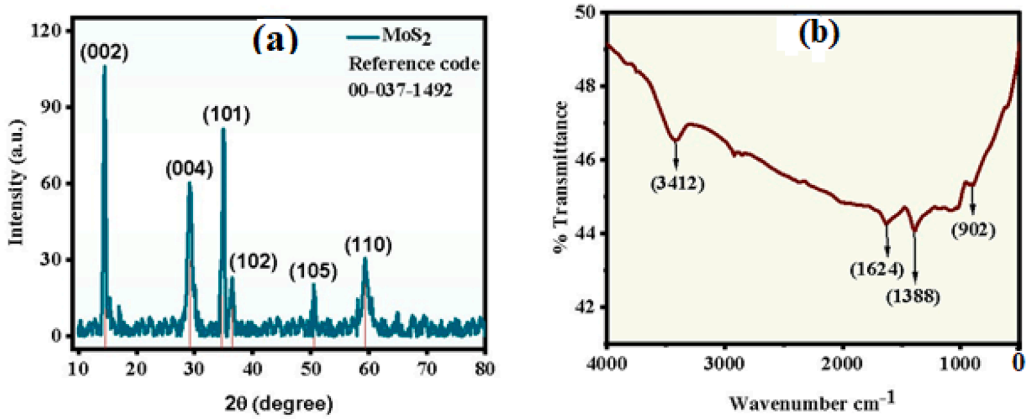

Fig. 3. (a) XRD spectrum of MoS_2 nanoflowers, (b) FT-IR spectrum of MoS_2 nanoflowers.

tronic properties of analytes and complex were carried out at cutoff energy of 500 eV. The long-range van der Waals interactions among GA and MoS_2 surface were explained by Grimme DFT-D2 method. We used a $4 \times 4 \times 1$ supercell for adsorption of GA. The vacuum of 25 Å was kept in z direction to avoid interaction between periodic sections. To obtain accurate results, convergence threshold of 10^{-5} along with convergence forces of 0.002 eV/ Å was utilized. In addition, self-consistent field (SCF) was set to 10^{-6} eV. The adsorption energy of GA on MoS_2 was calculated by the following Eq. (1).

$$E_{ads=E_{GA@MoS_2}-(E_{MoS_2}+E_{GA})} \quad (1)$$

Here, E_{ads}, $E_{GA@MoS_2}$, E_{MoS_2}, E_{GA} are adsorption energy, energy of GA@MoS_2 complex, and energy of GA, respectively.

3. Results and discussion

3.1. UV–Visible spectroscopic analysis

UV–Vis spectroscopy is regarded as a highly reliable and practical primary characterization tool for monitoring and determining the stability of synthesized nanoparticles. MoS_2 nanoparticles possess distinct optical characteristics that allow them to interact strongly with specific wavelengths of light. Particle size, chemical environment, and dielectric media all have a substantial effect on the absorption of MoS_2 nanoparticles. The UV–Vis spectrum of MoS_2 was measured at room temperature in the range of 200 to 800 nm, as revealed in Fig. 2(a). The absorption spectrum for MoS_2 nanoparticles was found at 218 nm, which was nearly identical to earlier research [32].

3.2. SEM/EDX analysis

Fig. 2 (b-c) depicts the surface morphology of the synthesized MoS_2 nanoparticles and it was observed that the particles were spherical in structure, had a flower-like appearance, and were highly porous in nature. The nanoflowers were arranged in layers of petals, which increased the active surface area and proved highly useful during the detection of the targeted analyte. The flower-like morphology was obviously responsible for providing extra active binding sites, allowing an accumulation of electrons that were easily transferred during the reaction to boost optical activity and electrical conductivity. The EDX spectrum of the elemental analysis for the MoS_2 nanoflowers, as shown in Fig. 2(d), readily demonstrated the occurrence of Molybdenum (Mo) and Sulphur (S). Without identifying contaminants, the elemental percentages of Mo and S in the nanoflowers were 50.8 % and 28 %, while Oxygen (O) of 21.2 %, respectively.

Table 1
Comparison of V_{maX} and K_M amongst MoS_2 nanoflowers and former catalysts.

Catalyst	Substrate	K_M (mM)	V_{maX} (10^{-8} M.s^{-1})	Refs.
HRP	TMB	0.434	10	[34]
	H_2O_2	3.7	8.71	
MoS_2-$Pt_{74}Ag_{26}$	TMB	0.386	3.22	[35]
	H_2O_2	25.71	7.29	
MoS_2@CNNS	TMB	0.117	3.03	[36]
	H_2O_2	0.602	3.15	
CTAB-MoS_2	TMB	6.92	4.54	[37]
	H_2O_2	0.022	0.223	
MoS_2 nanoflowers	TMB	0.892	3.44	Current work
	H_2O_2	0.13	2.98	

3.3. XRD and FTIR analysis

Fig. 3(a) describes the spectrum of XRD data of MoS_2 nanoparticles between 10° and 80° The diffraction peaks of MoS_2 were detected at 14.28°, 29.2°, 32.5°, 36.5°, 50.52°, and 59.3°, respectively, and were indexed with the crystal planes of (002), (004), (101), (102), (105) and (110). They are assigned to the nanostructure using JCPDS reference no. 037-1492. Debye-Scherrer's Eq. (2) was used to calculate the crystallite size of the MoS_2 nanoparticles, which was calculated to be 28 nm and therefore proven to be in the nanosized range.

$$D = K\lambda / \beta Cos\theta \quad (2)$$

Here, D represents crystal size, K is the Scherrer constant (0.98), signifies wavelength, and β denotes full width at half maximum.

The FT-IR spectrum of MoS_2 nanoparticles was noted in the range 4000 to 500 cm^{-1} to recognize the functional groups and chemical interactions present in MoS_2, as demonstrated in Fig. 3(b). The stretching vibrations for the S-S bond were attributed to the absorption band at 904 cm^{-1}, and the bands obtained at 1388 and 1630 cm^{-1} were associated with Mo-O and S-S vibrations. At maximum wavenumber, the stretching of the O—H band centered at 3412 cm^{-1} [33].

3.4. Steady state kinetics of MoS_2 nanoflowers

By using steady-state kinetics, the peroxidase-like catalytic activity of MoS_2 nanoflowers was investigated further. The kinetic study was calculated using the Michaelis-Menten Eq. (3);

$$V_\circ = V_{max} \times [S]/K_M(+[S]) \quad (3)$$

The curves for Michaelis-Menten were calculated by changing the amount of TMB or H_2O_2 though keeping the other constant. The Lineweaver-Burk plot was then used to calculate the highest initial velocity V_{maX} and Michaelis-Menten constant K_M. K_M is a significant factor

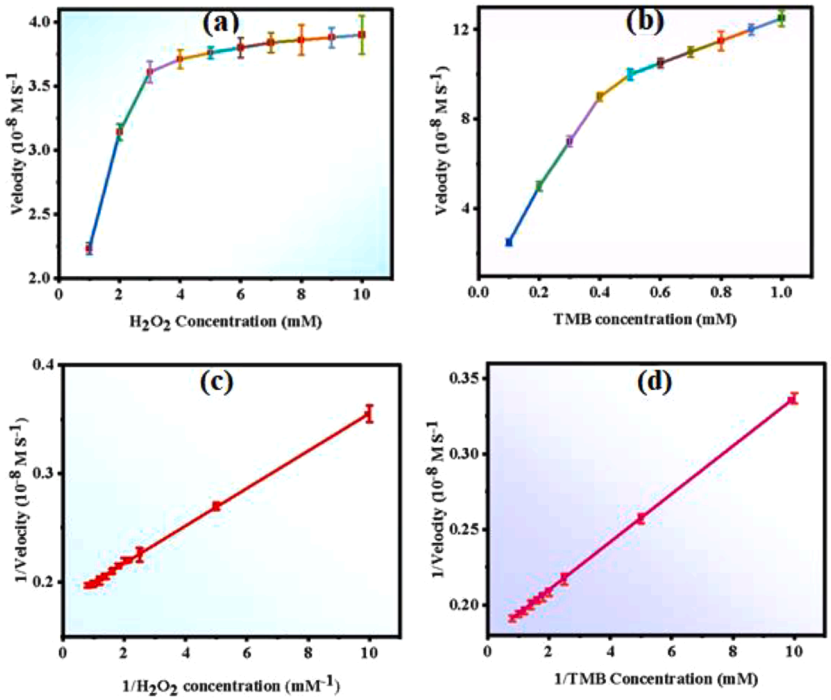

Fig. 4. Steady-state kinetic assay of MoS_2 nanoflowers: (a, b) 2 mM TMB with various amount of H_2O_2, (c, d) 5.0 mM H_2O_2 with various concentrations of TMB.

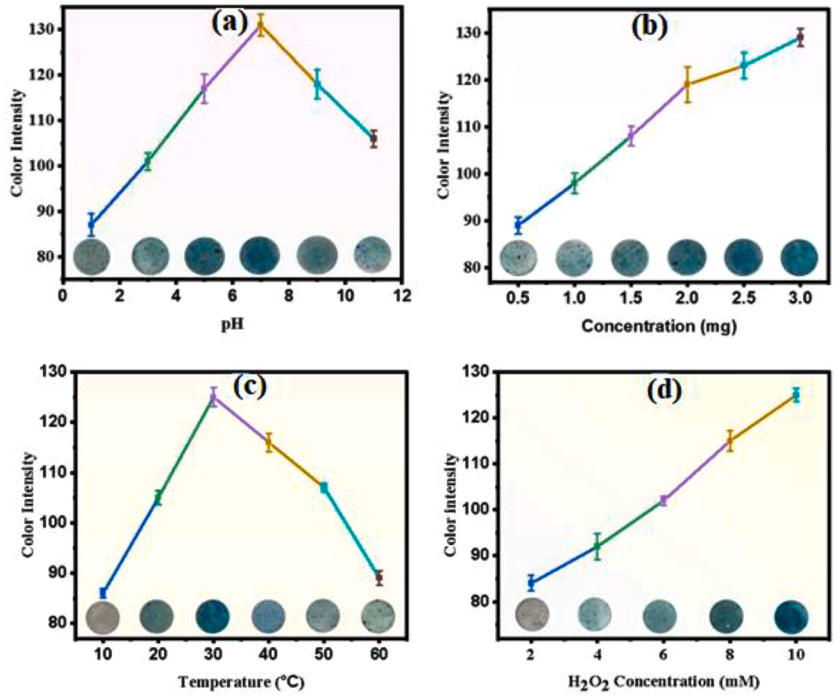

Fig. 5. The effect of (a) pH, (b) Concentration of MoS_2 nanoflowers, (c) Temperature, (d) Concentration of H_2O_2 on peroxidase-like activity.

that represents the affinity of an enzyme for its substrates, and [*S*] is the substrate concentration (TMB or H_2O_2) [28].

The Michaelis-Menten constant values for H_2O_2 and TMB were calculated to be as low as 0.13 and 0.829, respectively, indicating that the MoS_2 nanoflowers have a higher affinity for the substrate. Table 1 depicts previously reported literature; the V_{maX} value for the suggested sensing platform was greater than earlier work. The kinetic assay of MoS_2 nanoflowers is presented in Fig. 4, and it is clear that MoS_2 nanoflowers demonstrated strong catalytic activities in the presence of H_2O_2, leading us to conclude that MoS_2 nanoflowers could be a promising choice for GA colorimetric detection due to their peroxidase-like capabilities. According to Table 1, MoS_2 nanoflowers with H_2O_2 as substrate had a lower apparent K_M than the well-known HRP (natural enzyme), MoS_2-$Pt_{74}Ag_{26}$, and other MoS_2-based nanozymes, indicating that MoS_2 nanoflowers have the highest binding affinity towards H_2O_2. In contrast, the evident K_M value of MoS_2 using TMB as a substrate was greater than that of MoS_2@CNNS, HRP and MoS_2-$Pt_{74}Ag_{26}$.

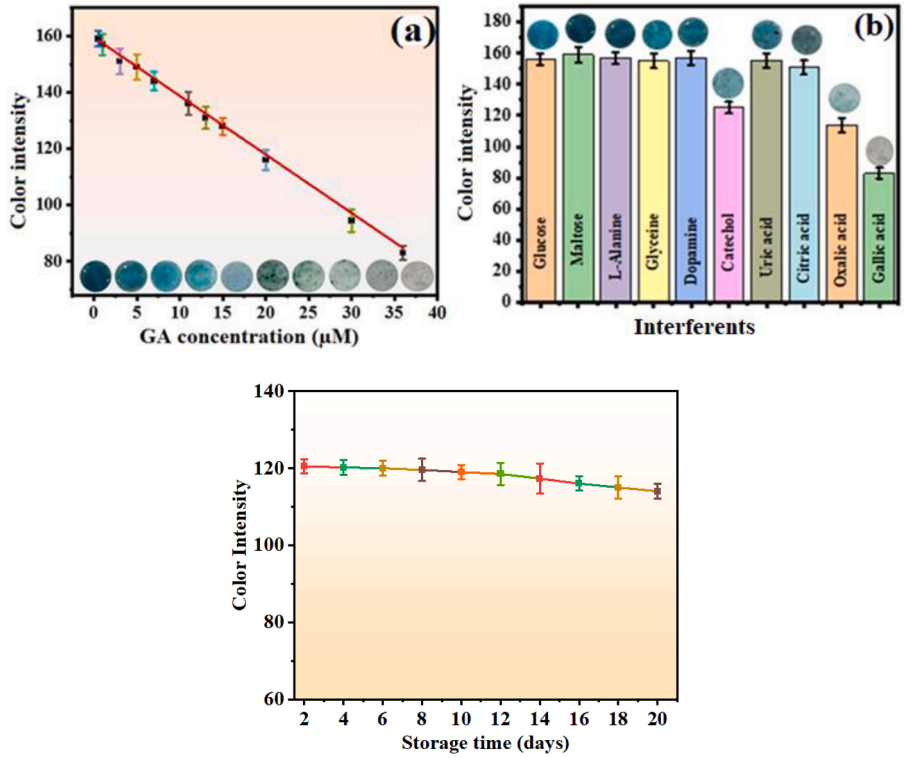

Fig. 6. (a) The curve of dose-response and naked-eye color intensity for GA sensing in the linear range of 0.5 to 36 × 10^{-6} M under optimum conditions, (b) Selectivity of the proposed sensor in the presence of various interfering species, (c) Stability of the proposed sensor.

3.5. Optimization studies

To determine the best ideal conditions for GA detection, many essential optimization parameters such as pH (1–12), reaction temperature (10 to 60 °C), and dosage of MoS_2 nanoparticles (0.5–3 mg) were examined. In the existence of H_2O_2, a typical chromogenic TMB reaction was carried out, which was catalyzed by MoS_2 nanoflowers and resulted in the conversion of colorless TMB to blue ox-TMB, as expected and observed with the naked eye. As a control, the individual reaction between TMB and H_2O_2 showed little response, but the addition of MoS_2 nanoflowers further enhanced the reaction owing to its strong peroxidase-like behavior. Fig. 5(a) demonstrated that by increasing the pH, the color intensity increased up to pH 7 and then steadily decreased; at pH 12, no activity was observed; thus, pH 7 was chosen as an optimal pH, indicating the possibility of TMB oxidation under normal conditions and potentially facilitating MoS_2 catalyzed H_2O_2 breakdown into radicals. The Fig. 5(a) showed, that the MoS_2 nanoflowers have a high catalytic activity in an extensive scale of pH (4.0–7.8), which was far-reaching than that of already testified peroxidase mimetics like; MIL-53(Fe) [38], TiO_2 nanotubes [39], Fe_3O_4 NPs [34] and $ZnFe_2O_4$ NPs [40].

Fig. 5(b,d) presents the effect of concentration of MoS_2 nanoflowers and H_2O_2 on peroxidase-like behavior; as per the concentration of MoS_2 nanoflowers and H_2O_2 concentration amplified, the color intensity rose as well, and after a certain limit, its concentration tended towards saturation. As a result, the optimal dosage of MoS_2 nanoflowers and H_2O_2 on peroxidase-like activity was found to be 2 mg and 6 mM respectively for GA detection, which was selected for subsequent studies.

Six filter sheets were stored at different temperatures (10, 20, 30, 40, 50, and 60°) for the detection of GA at optimal conditions. After thorough consideration at various intervals of time, the sensor at 30 °C was determined to be the most effective and ideal for ongoing study, as shown in Fig. 5(c).

Table 2
Comparison of the present work with the already-testified sensors for the detection of GA.

Sr. No	Materials	Linear range (μM)	LOD (10^{-6} M)	Refs.
1	[a]TNrGO	10–100	3.1	[41]
2	[b]SPCE/PME	1–1000	0.21	[42]
3	[c]NiO—OMC	0.2–10	0.112	[9]
4	[d]APLE	0.49–24.3	0.25	[43]
5	MoS_2 nanoflowers	0.5–36	0.125	Present work

[a] Titanium nitride doped reduced graphene oxide. [b]Screen-printed carbon electrode. [C]Nickel assembled at ordered mesoporous carbon. [d]Activated pencil lead electrode.

3.6. Calibration plot and sensitivity analysis for the detection of GA

GA is a type of phenolic compound that acts as a potent antioxidant and because of its reducibility; GA can change the color of ox-TMB from blue to colorless (Fig. 1). Under ideal conditions, in the presence of TMB and H_2O_2, GA was detected using MoS_2 nanoflowers as peroxidase-like mimics. As snatched in Fig. 6(a), the signal response of ox-TMB steadily decreased as the amount of GA increased. Furthermore, as seen with the naked eye, the equivalent color slowly transformed from deep blue to colorless. The limit of detection (LOD) for GA was determined in the range of 0.5–36 μM and was calculated to be as low as 0.125 × 10^{-6} M ($S/N = 3$) using the following formula:

$$\text{LOD} = 3.3\ \text{SD}/\text{Slop} \quad (4)$$

This detection limit was determined using the RGB model and did not correlate to the visual detection limit. With a correlation coefficient (R^2) of 0.993, the linear curve exhibited an appealing linear relationship. The RGB values of each concentration were calculated using an RGB color model. In comparison to previous GA sensing techniques (Table 2), the proposed colorimetric method platform was very acceptable in terms of

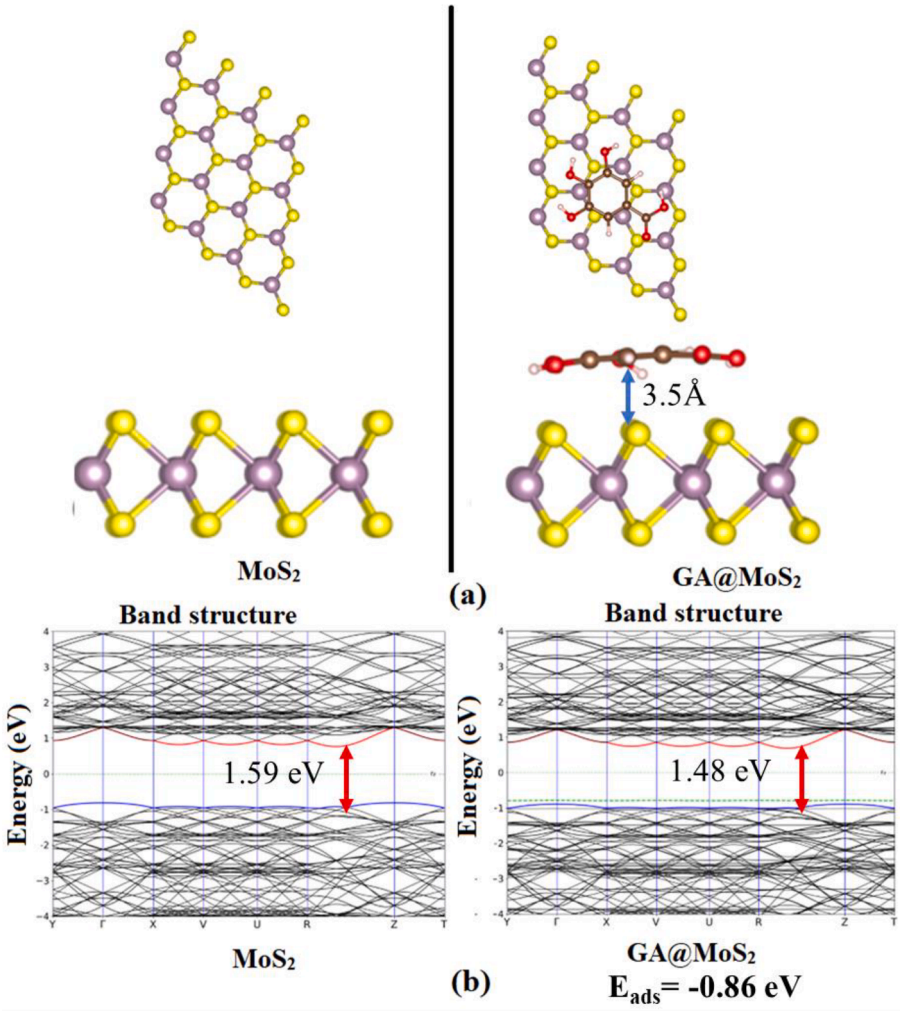

Fig. 7. (a) Top and side view of 4 × 4 × 1 supercell of MoS_2 and GA@MoS_2 complex, (b) Band structures of MoS_2 and GA@MoS_2 complexes.

low cost, direct visual dimensions, and low detection limit.

3.7. Selectivity and stability

The effect of some amino acids and other compounds on GA detection was investigated to determine the effect of possible interferants such as glucose, maltose, L-alanine, glycine, dopamine, catechol, uric acid, citric acid and ascorbic acid with concentration of 10 μM solution of each under already optimized conditions. As indicated in Fig. 6(b), the only colorless solution was obtained for GA which was applied in the concentration of 10 μM solution. As a result, it was demonstrated that the suggested sensing platform was greatly selective and well-suited for the rapid determination of GA in the presence of multiple other analytes and could be devised for measuring GA on the spot.

The stability of the developed sensor was observed by the changes in the intensity of the color in response of MoS_2 nanoparticles to GA under optimized conditions after the storage of 20 days at room temperature. As a result, it may be noted that negligible or very small change was observed in performance of the proposed sensor Fig. 6(c). Therefore, the proposed paper based colorimetric detection assay towards the targeted analyte using MoS_2 nanoparticles have reasonable and better stability as compared to other reported work [44] with RSD value less than 5 %.

3.8. Computational analysis

In the current study, we used a 4 × 4 × 1 supercell of MoS_2 as sensor surface for detection of GA with lattice constant of 12.76 Å. The bond length between Mo-S observed was 2.4 Å, while S-S bond length was 3.1 Å, which was consistent with prior studies [45]. The adsorption of GA over MoS_2 was tested through several orientations in order to obtain a stable GA@MoS_2 complex. Each time, we obtained approximately the same orientation, where GA being absorbed in a parallel orientation over MoS_2. In parallel adsorption, the maximum number of GA atoms interacted with S-atoms of MoS_2 (Fig. 7(a)). The adsorption distance of 3.5 Å was observed between atoms of GA and the S-atoms of MoS_2 surface. However, the adsorption energy for GA@MoS_2 complex was-0.86 eV. The values of adsorption energy and adsorption distance revealed the physisorption of GA over MoS_2.

3.9. Electronic properties

The selectivity and sensitivity of GA by MoS_2 was evaluated by band analysis. The band structures of MoS_2 and GA@MoS_2 complex are presented in the Fig. 7(b). For bare of 4 × 4 × 1 supercell of MoS_2, the values of conduction band maximum and valence band minimum (VBM) were 0.76 eV and -0.82 eV with band gap energy of 1.59 eV (Table 3). This showed that MoS_2 is direct band semiconductor, which was comparable to previous studies [46]. The adsorption of GA brought potential decreases in energies of VBM (−0.79 eV) and CBM (0.69 eV) with band energy gap of 1.48 eV compared to bare MoS_2 (1.59 eV). In addition, changes in band structures were also noted before and after adsorption of GA over MoS_2. These findings displayed that adsorption of GA over

Table 3
The energies of valance band maximum (eV), conduction band minimum (eV) and band energy gap.

Complex	Valance band (eV)	Conduction band (eV)	Band energy gap (eV)
MoS_2	−0.82	0.76	1.59
GA@MoS_2	−0.79	0.69	1.48

Table 4
Real time application of proposed sensor for GA detection.

Samples	GA spiked (μM)	GA found (μM)	Relative% recovery
Blood serum	5	4.94	98.4 ± 0.2
	10	9.51	95.1 ± 0.3
	15	14.33	95.5 ± 0.4
Urine	5	4.76	95.2 ± 0.3
	10	9.32	93.2 ± 0.2
	15	14.29	95.2 ± 0.3
Tap water	5	4.79	95.8 ± 0.3
	10	9.52	95.2 ± 0.4
	15	14.44	96.2 ± 0.2
Green tea	5	5.09	100.8 ± 0.3
	10	10.21	102.1 ± 0.4
	15	15.14	100.9 ± 0.3
Diet tea	5	5.03	100.6 ± 0.2
	10	10.11	101.1 ± 0.3
	15	15.23	101.53 ± 0.2

MoS_2 resulted in a significant increase in conductivity of GA@MoS_2 complex compared to bare MoS_2. Thus, it is concluded that MoS_2 can act as potential sensor for the detection of GA.

3.10. Real sample analysis

To test the capability and reliability of the proposed sensing platform in complex real-world media, biological samples (blood serum and urine), food samples (green tea and diet tea), and environmental samples were used. The proposed sensing platform responded to GA efficiently in the spiked samples. The percentage recoveries were found to be in the 93.2–102.1 % range. The results in Table 4 confirmed the sensor's reliability and suggested the idea of a portable device for one-to-one care in biological and environmental applications.

4. Conclusion

In the current study, we successfully developed a colorimetric detection method based on MoS_2 nanoparticles acting as nanozymes for sensitive and selective measurement of GA. The as-synthesized material was characterized using a number of analytical techniques that properly supported the detection approach. During the detection process, MoS_2 nanoflowers performed as a peroxidase-like nanozyme, whereas GA acted as a reducer, inhibiting the system's color change. Under optimal conditions of pH, temperature, MoS_2, and H_2O_2 concentrations, the proposed platform displayed a very low limit of detection across a wider range. Furthermore, the suggested GA sensor displayed exceptional anti-interference capabilities in the presence of a variety of strong interfering species and great stability aswell. Calculations using density functional theory at the PBE functional of GGA revealed that GA was physiosorbed on MoS_2 with interaction energy of 0.86 eV. The band gap research indicated that following GA adsorption on MoS_2, the band gap reduced to 1.48 eV compared to 1.59 eV for the bare MoS_2 surface. It was determined that by quenching the peroxidase-like action of MoS_2 nanoflowers, a highly accurate, selective, and sensitive colorimetric GA sensing approach could be exploited. The proposed sensor has a high potential for portability for onsite GA detection, as reflected by its real-world application in complex media.

CRediT authorship contribution statement

Aizaz Khan: Formal analysis, Writing – original draft. **Huma Ajab:** Writing – review & editing, Supervision, Methodology, Conceptualization. **Asim Yaqub:** Data curation, Methodology. **Khurshid Ayub:** Software, Visualization. **Muhammad Yar:** Data curation, Software. **Habib Ullah:** Software, Validation.

Declaration of competing interest

The authors declare that they have no known competing financial interests or personal relationships that could have appeared to influence the work reported in this paper.

Data availability

No data was used for the research described in the article.

References

[1] F.H.A. Fernandes, H.R.N. Salgado, Gallic acid: review of the methods of determination and quantification, Crit. Rev. Anal. Chem. 46 (2016) 257–265, https://doi.org/10.1080/10408347.2015.1095064.
[2] M. Sivakumar, K. Pandi, S.M. Chen, S. Yadav, T.W. Chen, V. Veeramani, Highly sensitive detection of gallic acid in food samples by using robust $NiAl_2O_4$ nanocomposite materials, J. Electrochem. Soc. 166 (2019) B29, https://doi.org/10.1149/2.0121902jes.
[3] B. Bajpai, S. Patil, A new approach to microbial production of gallic acid, Braz. J. Microbiol. 39 (2008) 708–711, https://doi.org/10.1590/S1517-83822008000400021.
[4] E. Alipour, F. Mirzae Bolali, S. Norouzi, A. Saadatirad, Electrochemically activated pencil lead electrode as a sensitive voltammetric sensor to determine gallic acid, Food Chem. 375 (2022) 131871, https://doi.org/10.1016/j.foodchem.2021.131871.
[5] K. Narumi, J.I. Sonoda, K. Shiotani, M. Shigeru, M. Shibata, A. Kawachi, E. Tomishige, K. Sato, T. Motoya, Simultaneous detection of green tea catechins and gallic acid in human serum after ingestion of green tea tablets using ion-pair high-performance liquid chromatography with electrochemical detection, J. Chromatogr. B 945-946 (2014) 147–153, https://doi.org/10.1016/j.jchromb.2013.11.007.
[6] J. Pooralhossini, M. Ghaedi, M.A. Zanjanchi, A. Asfaram, The choice of ultrasound assisted extraction coupled with spectrophotometric for rapid determination of gallic acid in water samples: central composite design for optimization of process variables, Ultrason. Sonochem. 34 (2017) 692–699, https://doi.org/10.1016/j.ultsonch.2016.07.003.
[7] W. Phakthong, B. Liawruangrath, S. Liawruangrath, Determination of gallic acid with rhodanine by reverse flow injection analysis using simplex optimization, Talanta 130 (2014) 577–584, https://doi.org/10.1016/j.talanta.2014.06.024.
[8] L. Han, P. Liu, H. Zhang, F. Li, A. Liu, Phage capsid protein-directed MnO_2 nanosheets with peroxidase-like activity for spectrometric biosensing and evaluation of antioxidant behaviour, ChemComm 53 (2017) 5216–5219, 1.10039/c7cc020449j.
[9] L. Yan, H. Ren, Y. Guo, G. Wang, C. Liu, Y. Wang, X. Liu, L. Zeng, A. Liu, Rock salt type NiO assembled on ordered mesoporous carbon as peroxidase mimetic for colorimetric assay of gallic acid, Talanta 201 (2019) 406–412, https://doi.org/10.1016/j.talanta.2019.04.025.
[10] Z. Chen, Z. Zhang, J. Qi, J. You, J. Ma, L. Chen, Colorimetric detection of heavy metal ions with various chromogenic materials: strategies and applications, J. Hazard. Mater. 441 (2023) 129889, https://doi.org/10.1016/j.jhazmat.2022.129889.
[11] P. Worramongkona, K. Seeda, P. Phansomboon, N. Ratnarathorn, O. Chailapakul, W. Dungchai, A simple paper-based colorimetric device for rapid and sensitive urinary oxalate determinations, Anal. Sci. 34 (2018) 103–108, https://doi.org/10.2116/analsci.34.103.
[12] I. Ullah, A. Yaqub, M.Z.U. Haq, H. Ajab, A.T. Jafry, M.K. Khan, Sensitive and cost-effective colorimetric sensor based on enzyme mimic MoS_2@ $CoTiO_3$ nanocomposite for detection of hydrogen peroxide in milk and tap water, J. Food Compost. Anal. (2023) 105689, https://doi.org/10.1016/j.jfca.2023.105689.
[13] Y. Cai, L. Niu, X. Liu, Y. Zhang, Z. Zheng, L. Zeng, A. Liu, Hierarchical porous MoS_2 particles: excellent multi-enzyme-like activities, mechanism and its sensitive phenol sensing based on inhibition of sulfite oxidase mimics, J. Hazard. Mater. 425 (2022) 128053, https://doi.org/10.1016/j.jhazmat.2021.128053.
[14] X. Zhang, Z. Lin, Y. Cai, X. Liu, L. Niu, A. Liu, Selective and sensitive colorimetric sensing of iodine ions based on porous MoS_2 particles with excellent haloperoxidase-like activity, Sens. Actuators B Chem. 392 (2023) 134127, https://doi.org/10.1016/j.snb.2023.134127.
[15] M. Buzdar, A. Yaqub, A. Hayat, M.Z.U. Haq, A. Khan, H. Ajab, Paper based colorimetric sensor using novel green magnetized nanocomposite of pinus for

hydrogen peroxide detection in water and milk, Food Biosci. 55 (2023) 103014, https://doi.org/10.1016/j.fbio.2023.103014.
[16] T. Naganuma, Shape design of cerium oxide nanoparticles for enhancement of enzyme mimetic activity in therapeutic applications, Nano Res. 10 (2017) 199–217, https://doi.org/10.1007/s12274-016-1278-4.
[17] X. Wang, W. Guo, Y. Hu, J. Wu, H. Wei, Nanozymes: Next Wave of Artificial Enzymes, X. Wang, W. Guo, Y. Hu, J. Wu, H. Wei (Eds.), Springer Berlin Heidelberg, Berlin, Heidelberg, 2016, pp. 7–29, https://doi.org/10.1007/978-3-662-53068-9_2.
[18] T.F. Jaramillo, K.P. Jørgensen, J. Bonde, J.H. Nielsen, S. Horch, I. Chorkendorff, Identification of active edge sites for electrochemical H_2 evolution from MOS_2NANOCATALYSTS, Science 317 (2007) 100–102, https://doi.org/10.1126/science.11414.
[19] D. Zhang, Z. Yang, P. Li, M. Pang, Q. Xue, Flexible self-powered high-performance ammonia sensor based on Au-decorated $MoSe_2$ nanoflowers driven by single layer MoS_2-flake piezoelectric nanogenerator, Nano Energy 65 (2019) 103974, https://doi.org/10.1016/j.nanoen.2019.103974.
[20] X. Guo, Y. Wang, F. Wu, Y. Ni, S. Kokot, A colorimetric method of analysis for trace amounts of hydrogen peroxide with the use of the nano-properties of molybdenum disulfide, Analyst 140 (2015) 1119–1126, https://doi.org/10.1039/C4AN01950D.
[21] Z. Tang, Q. Wei, B. Guo, A generic solvent exchange method to disperse MoS_2 in organic solvents to ease the solution process, ChemComm 50 (2014) 3934–3937, https://doi.org/10.1039/C4CC00425F.
[22] T. Lin, L. Zhong, L. Guo, F. Fu, G. Chen, Seeing diabetes: visual detection of glucose based on the intrinsic peroxidase-like activity of MoS_2 nanosheets, Nanoscale 6 (2014) 11856–11862, https://doi.org/10.1039/C4NR03393K.
[23] Q. Wang, X. Zhang, L. Huang, Z. Zhang, S. Dong, One-pot synthesis of Fe_3O_4 nanoparticle loaded 3D porous graphene nanocomposites with enhanced nanozyme activity for glucose detection, ACS Appl. Mater. Interfaces 9 (2017) 7465–7471, https://doi.org/10.1021/acsami.6b16034.
[24] M. Tang, D. Zhang, D. Wang, J. Deng, D. Kong, H. Zhang, Performance prediction of 2D vertically stacked MoS_2-WS_2 heterostructures base on first-principles theory and Pearson correlation coefficient, Appl. Surf. Sci. 596 (2022) 153498, https://doi.org/10.1016/j.apsusc.2022.153498.
[25] D. Zhang, S. Yu, X. Wang, J. Huang, W. Pan, J. Zhang, B.E. Meteku, J. Zeng, UV illumination-enhanced ultrasensitive ammonia gas sensor based on (001)TiO_2/MXene heterostructure for food spoilage detection, J. Hazard. Mater. 423 (2022) 127160, https://doi.org/10.3390/w14071073.
[26] Z. Liu, Y. Gui, L. Xu, X. Chen, Adsorption and sensing performances of transition metal (Ag, Pd, Pt, Rh, and Ru) modified WSe2 monolayer upon SF6 decomposition gases (SOF2 and SO2F2), Appl. Surf. Sci. 581 (2022) 152365, https://doi.org/10.1016/j.apsusc.2021.152365.
[27] F. Wang, G. Li, J. Zheng, J. Ma, C. Yang, Q. Wang, Hydrothermal synthesis of flower-like molybdenum disulfide microspheres and their application in electrochemical supercapacitors, RSC Adv. 8 (2018) 38945–38954, https://doi.org/10.1039/C8RA04350G.
[28] X. Zheng, Q. Lian, L. Zhou, Y. Jiang, J. Gao, Peroxidase mimicking of binary polyacrylonitrile-CuO nanoflowers and the application in colorimetric detection of H_2O_2 and ascorbic acid, ACS Sustain. Chem. Eng. 9 (2021) 7030–7043, https://doi.org/10.1021/acssuschemeng.1c00723.
[29] H. Ren, X. Liu, L. Yan, Y. Cai, C. Liu, L. Zeng, A. Liu, Ocean green tide derived hierarchical porous carbon with bi-enzyme mimic activities and their application for sensitive colorimetric and fluorescent biosensing, Sens. Actuators B Chem. 312 (2020) 127979, https://doi.org/10.1016/j.snb.2020.127979.
[30] X. Liu, L. Yan, H. Ren, Y. Cai, C. Liu, L. Zeng, J. Guo, A. Liu, Facile synthesis of magnetic hierarchical flower-like Co_3O_4 spheres: mechanism, excellent tetra-enzyme mimics and their colorimetric biosensing applications, Biosens. Bioelectron. 165 (2020) 112342, https://doi.org/10.1016/j.bios.2020.112342.
[31] H. Ren, L. Yan, M. Liu, Y. Wang, X. Liu, C. Liu, K. Liu, L. Zeng, A. Liu, Green tide biomass templated synthesis of molybdenum oxide nanorods supported on carbon as efficient nanozyme for sensitive glucose colorimetric assay, Sens. Actuators B Chem. 296 (2019) 126517, https://doi.org/10.1016/j.snb.2019.04.148.
[32] Y. Chen, L. Tan, M. Sun, C. Lu, J. Kou, Z. Xu, Enhancement of photocatalytic performance of TaON by combining it with noble-metal-free MoS_2 cocatalysts, J. Mater. Sci. 54 (2019) 5321–5330, https://doi.org/10.1007/s10853-018-03214-9.
[33] H. Ganesha, S. Veeresh, Y.S. Nagaraju, M. Vandana, M. Basappa, H. Vijeth, H. Devendrappa, 2-Dimensional layered molybdenum disulfide nanosheets and CTAB-assisted molybdenum disulfide nanoflower for high performance supercapacitor application, Nanoscale Adv. 4 (2022) 521–531, https://doi.org/10.1039/D1NA00664A.
[34] L. Gao, J. Zhuang, L. Nie, J. Zhang, Y. Zhang, N. Gu, T. Wang, J. Feng, D. Yang, S. Perrett, Intrinsic peroxidase-like activity of ferromagnetic nanoparticles, Nat. Nanotechnol. 2 (2007) 577–583, https://doi.org/10.1038/nnano.2007.260.
[35] S. Cai, Q. Han, C. Qi, Z. Lian, X. Jia, R. Yang, C. Wang, Pt 74 Ag 26 nanoparticle-decorated ultrathin MoS_2 nanosheets as novel peroxidase mimics for highly selective colorimetric detection of H_2O_2 and glucose, Nanoscale 8 (2016) 3685–3693, https://doi.org/10.1039/C5NR08038J.
[36] P. Ju, Y. He, M. Wang, X. Han, F. Jiang, C. Sun, C. Wu, Enhanced peroxidase-like activity of MoS_2 quantum dots functionalized g-C_3N_4 nanosheets towards colorimetric detection of H_2O_2, Nanomater 8 (2018) 976, https://doi.org/10.3390/nano8120976.
[37] G. Tang, J. Sun, C. Wei, K. Wu, X. Ji, S. Liu, H. Tang, C. Li, Synthesis and characterization of flowerlike MoS_2 nanostructures through CTAB-assisted hydrothermal process, Mater. Lett. 86 (2012) 9–12, https://doi.org/10.1016/j.matlet.2012.07.014.
[38] L. Ai, L. Li, C. Zhang, J. Fu, J. Jiang, MIL-53 (Fe): a metal-organic framework with intrinsic peroxidase-like catalytic activity for colorimetric biosensing, Chem. Eur. J. 19 (2013) 15105–15108, https://doi.org/10.1002/chem.201303051.
[39] L. Zhang, L. Han, P. Hu, L. Wang, S. Dong, TiO_2 nanotube arrays: intrinsic peroxidase mimetics, Chem. Commun. 49 (2013) 10480–10482, https://doi.org/10.1039/C3CC46163G.
[40] L. Su, J. Feng, X. Zhou, C. Ren, H. Li, X. Chen, Colorimetric detection of urine glucose based $ZnFe_2O_4$ magnetic nanoparticles, Anal. Chem. 84 (2012) 5753–5758, https://doi.org/10.1021/ac300939z.
[41] D.M. Stanković, M. Ognjanović, F.Ľ. Martin Švorc, J.F. Mariano, B. Antić, Design of titanium nitride-and wolfram carbide-doped RGO/GC electrodes for determination of gallic acid, Anal. Biochem. 539 (2017) 104–112, https://doi.org/10.1016/j.ab.2017.10.018.
[42] Y.L. Su, S.H. Cheng, Sensitive and selective determination of gallic acid in green tea samples based on an electrochemical platform of poly (melamine) film, Anal. Chim. Acta 901 (2015) 41–50, https://doi.org/10.1016/j.aca.2015.10.026.
[43] E. Alipour, F.M. Bolali, S. Norouzi, A. Saadatirad, Electrochemically activated pencil lead electrode as a sensitive voltammetric sensor to determine gallic acid, Food Chem. 375 (2022) 131871, https://doi.org/10.1016/j.foodchem.2021.131871.
[44] S.E. Bustamante, S. Vallejos, B.S.P. Portal, A. Muñoz, A. Mendia, B.L. Rivas, F. C. García, J.M. Garcia, Polymer films containing chemically anchored diazonium salts with long-term stability as colorimetric sensors, J. Hazard. Mater. 365 (2019) 725–732, https://doi.org/10.1016/j.jhazmat.2018.11.066.
[45] I. Ahmad, S.A. Khan, M. Idrees, M. Haneef, I. Shahid, H.U. Din, S.A. Khan, B. Amin, Influence of strain on specific features of MoX_2 (X= S, Se, Te) monolayers, Phys. B Condens. 545 (2018) 113–118, https://doi.org/10.1016/j.physb.2018.05.034.
[46] E. Salih, A.I. Ayesh, First principle study of transition metals codoped MoS_2 as a gas sensor for the detection of NO and NO_2 gases, Phys. E Low Dimens. Syst. Nanostruct. 131 (2021) 114736, https://doi.org/10.1016/j.physe.2021.114736.